Supplement of Atmos. Chem. Phys., 26, 8341–8353, 2026
https://doi.org/10.5194/acp-26-8341-2026-supplement

Atmospheric Chemistry and Physics
Open Access

Supplement of

Marine-derived water-soluble organic nitrogen in coastal air: influence of ocean productivity on atmospheric nitrogen cycling

Jiao Tang et al.

Correspondence to: Shujie Hu (hushujie@cigit.ac.cn) and Shizhen Zhao (zhaoshizhen@gig.ac.cn)

Text S1. PMF model

Data Input

The data input includes concentrations and uncertainties of various types of chemicals in 84 TSP samples. The types of chemicals include WSON, OC, EC, metal elements (Ni, V, Pb, Cu, Zn, Mn, Fe, Al), water-soluble ions (K^+, Na^+, Mg^{2+}, Ca^{2+}, NH_4^+, Cl^-, SO_4^{2-}, NO_3^-), biomass burning tracers (levoglucosan, mannosan, galactosan), steranes, hopanes, and SOA tracers (2-MGA, 2MGL, MBTCA, o/p-phthalic acid). The uncertainty file provides species-specific parameters that EPA PMF 5.0 uses to calculate uncertainties for each sample. If the concentration is less than or equal to the method detection limit (MDL), the uncertainty (Unc) is calculated using a fixed fraction of the MDL (1), and the concentration is replaced with half of the MDL.

$$Unc = \frac{5}{6} \times MDL \quad (1)$$

If the concentration is higher than the MDL, the calculation is based on a user- provided fraction of the concentration and MDL (Equation 2). Al element was set as bad, resulting in solutions that didn't converge. Weak signals were found for species of galactosan, mannosan, levoglucosan, hopanes and steranes, 2-MGA, and o-Phthalic acid, which had a low signal-to-noise ratio (S/N<3). Other species with an S/N greater than 3 were set as strong.

$$Unc = \sqrt{(\text{Error Fraction} \times \text{concentrations})^2 + (0.5 \times MDL)^2} \quad (2)$$

Model run

The PMF model was executed using three to seven factors, 100 runs, and a random starting point, resulting in converged solutions. Despite yielding the lowest Q_{robust}/Q_{true} ratio (1.043, approaching unity), the six-factor solution exhibited mixing of the NH_4^+ and SO_4^{2-} with biomass burning tracers. This chemically implausible separation rendered the six-factor interpretation problematic. Consequently, the seven-factor solution was selected for source profile analysis as it provided physically meaningful resolution.

For WSON was set as the total variable:

Uncertainty Estimation: To understand the uncertainty of the seven-factor solution, we did a complementary analysis of displacement (DISP), BS, and bootstrapping with displacement (BS-DISP). We used DISP intervals to include the effects of rotational ambiguity, but not the effects of random errors in the data. BS intervals included the effects of random errors and partially included the effects of rotational ambiguity. Finally, BS-DISP intervals included the effects of both random errors and rotational ambiguity. Tables S4–S5 show that the seven-factor solutions for WSON do not have significant

rotational ambiguity, and the base model and error estimates can be interpreted. With the absence of any swaps, dQ_{max} provides confidence that these solutions are well constrained.

As shown in Figure S8, factor 1 was linked to high contribution of V, suggesting that it came from a shipping emission source (Celo et al., 2015; Viana et al., 2009). Factor 2 was characterized by high levels of NH_4^+ and SO_4^{2-}, which was a secondary sulfate source. Factor 3 (dust) showed a high contribution of Mn (69 %), Fe, Mg^{2+}, and Ca^{2+}. Factor 4 was identified as SOA source because it was associated with high loadings of 2-MGA, 2-MGL, MBTCA, and p-phthalic acid. Factor 5 was linked to biomass burning, with high loadings of galactosan, mannosan, and levoglucosan, NH_4^+, NO_3^-, and p-phthalic acid also had high loading for this source, as reported in the source profiles of biomass burning (Li et al., 2007). Factor 6 showed high loadings with Pb, Cu, and Zn and was identified as vehicle emissions and fossil fuel combustion. Factor 7 was associated with high levels of Na^+, Cl^-, and Mg^{2+}, which was identified as sea spray aerosols via the bubble-busting processes (Facchini et al., 2008).

Text S2. Potential Source Contribution Function (PSCF) Model

The PSCF model facilitates the identification of source region by partitioning the potential source domain into a grid matrix of $i \times j$, as detailed in our previous study (Geng et al., 2020; Tang et al., 2024). The PSCF analysis typically generates $PSCF_{ij}$ values ranging from 0 to 1, with elevated $PSCF_{ij}$ suggesting an increased likelihood that the ij_{th} cell being the source region. A notable constraint of PSCF-based methodologies is the necessity to establish a weighing function to designed to diminish the influences of cells with minimal residence time, a phenomenon often manifested as “trailing effects” (Petit et al., 2017). To investigate the partitioning of aerosol sources and to ascertain the contributions of various aerosol emission sources and transportation mechanisms, we conducted a weighted Potential Source Contribution Function (WPSCF) analysis. Given that PSCF represents a conditional probability, the associated error escalates with increased distance between the grid and the sample points (Tiwari et al., 2018). In this investigation, the experimental area was divided into a 0.25°×0.25° grid. The threshold for the computation of m_{ij} was established at the 75th percentile. To mitigate the impact of small n_{ij} values on PSCF, a weighting function was applied (Tiwari et al., 2018):

$$w_{ij} = \begin{cases} 1.00 & n_{ij} > 80 \\ 0.70 & 20 < n_{ij} \leq 80 \\ 0.42 & 10 < n_{ij} \leq 20 \\ 0.05 & n_{ij} \leq 10 \end{cases} \quad (3)$$

Text S3. Predicting ALWC Using a Thermodynamic Model

To predict the mass concentration of aerosol liquid water content (ALWC), we used a

thermodynamic model, ISORROPIA-II, http://nenes.eas.gatech.edu/ISORROPIA/, which calculates the ALW concentration with particle-phase concentrations of Na^+, SO_2^-, NH_4^+, NO_3^-, Cl^-, Ca^{2+}, K^+, and Mg^{2+}, as well as meteorological conditions (RH and ambient temperature) as the input (Fountoukis and Nenes, 2007), which was described in our previous studies (Xu et al., 2022). Briefly, the contributions of particle water associated with organic fractions to ALW were estimated by calculating the organic hygroscopicity parameter. ALW was calculated as the sum of water associated with individual aerosol chemical components (i.e., the sum of ions and lumped organics) based on the Zdanovskii−Stokes−Robinson (ZSR) relationship.

Table S1. The concentrations of TSP, OC, EC, WSON, NH_4^+-N, NO_3^--N, and the ratios of OC/EC and WSON/WSON. In addition, the meteorological data, including relative humidity (RH), wind speed (WS), and temperature (Temp.) were also presented. Precipitation and radiation data are obtained from historical reanalysis datasets from European Centre for Medium-Range Weather Forecasts (ECMWF). Cluster indicates the air masses analyzed by HYSPLIT in Figures 1b and S1–S2.

Date	TSP (μg m^{-3})	OC (μg m^{-3})	EC (μg m^{-3})	OC/EC	WSON (μgN m^{-3})	NH_4^+-N (μgN m^{-3})	NO_3^--N (μgN m^{-3})	RH (%)	WS (mph)	Temp. (°C)	Precipitation (mm)	Radiation (W m^{-2})	Cluster
2016/1/18	42	10	1.7	6.1	0.31	0.11	0.55	80	5.6	29	0.453	2845.62	1
2016/1/25	66	19	1.4	13	0.73	0.32	0.73	65	11	17	0.049	456.26	3
2016/2/1	97	18	2.4	7.7	1.2	0.34	1.6	75	4.3	30	0.264	4340.11	1
2016/2/8	161	38	2.8	14	1.1	2.2	2.7	43	7.8	21	0.000	8144.62	5
2016/2/15	88	15	1.9	8.0	1.3	0.28	1.1	76	5.8	30	0.115	3605.48	1
2016/2/22	60	11	1.8	5.9	0.89	0.58	1.3	74	6.7	29	0.017	3355.82	2
2016/2/29	118	23	1.9	12	1.3	1.1	0.69	48	5.0	29	0.000	4671.43	3
2016/3/4	101	13	1.6	8.1	1.3	0.40	0.75	71	6.8	30	0.004	4642.70	1
2016/3/8	47	8.7	1.3	6.7	0.35	0.51	0.98	74	9.2	30	0.094	4934.61	2
2016/3/10	37	9.7	1.6	6.0	0.50	0.34	0.58	78	7.5	30	0.000	4929.85	2
2016/3/14	33	8.0	1.3	6.2	0.49	0.10	0.45	73	7.8	31	0.000	5116.68	2
2016/3/16	40	9.9	1.4	7.3	0.41	0.22	0.56	69	9.7	31	0.005	5223.13	2
2016/3/18	59	10	1.4	7.5	0.71	0.52	0.50	74	9.4	31	0.001	5809.82	2
2016/3/20	51	8.0	1.0	7.9	0.60	0.48	0.44	74	11	31	0.000	5953.51	2
2016/3/22	80	13	1.6	8.1	0.91	0.75	0.34	74	9.0	31	0.000	7301.90	2
2016/3/24	111	15	1.7	8.9	0.65	1.26	0.55	64	7.3	32	0.000	6984.91	1
2016/3/26	54	11	1.2	9.3	0.80	0.71	0.78	59	8.3	30	0.184	3269.41	3

2016/3/28	111	24	2.1	12	1.2	2.10	2.7	68	7.1	29	0.016	2870.25	4
2016/3/30	57	11	1.4	7.6	0.84	0.54	0.94	77	6.2	30	1.276	3838.34	2
2016/4/1	43	8.3	1.3	6.2	0.54	0.39	0.82	71	8.7	31	0.278	4539.01	2
2016/4/3	18	6.1	0.83	7.3	0.57	0.35	0.39	68	8.7	31	0.012	4226.13	2
2016/4/5	28	6.9	1.1	6.2	0.64	0.13	0.39	69	8.8	32	0.168	5370.84	2
2016/4/7	35	8.7	1.2	7.2	0.57	0.31	0.32	72	10	32	0.064	3968.69	2
2016/4/9	25	5.4	0.95	5.7	0.53	0.09	0.24	67	10	32	0.012	5640.03	2
2016/4/13	63	8.7	1.3	6.6	0.59	1.8	0.28	55	9.8	33	0.000	6572.45	1
2016/4/15	37	7.1	0.95	7.5	0.41	1.1	0.12	65	9.8	33	0.224	5262.17	2
2016/4/17	32	7.9	0.16	49	0.27	1.1	0.10	71	9.7	33	0.544	5817.36	2
2016/4/19	26	6.2	1.1	5.9	0.41	0.57	0.12	68	9.7	32	0.448	5535.08	2
2016/4/21	34	6.6	0.91	7.2	0.57	0.07	0.41	63	9.9	32	0.372	4912.19	2
2016/4/23	38	8.4	0.99	8.5	0.92	0.08	0.35	65	10	33	0.311	5393.97	2
2016/4/25	40	9.8	1.1	8.6	0.98	0.35	0.26	69	9.7	33	0.218	5708.40	2
2016/4/27	47	11	1.2	8.5	1.2	0.53	0.44	69	9.7	33	0.438	4995.66	2
2016/4/29	29	7.1	1.0	7.1	0.84	0.36	0.16	72	9.1	33	0.152	4496.61	2
2016/5/1	20	5.4	0.96	5.6	0.84	0.23	0.20	74	6.4	30	0.580	4786.53	1
2016/5/3	23	5.7	1.3	4.3	0.77	0.31	0.18	63	8.5	33	0.443	5948.07	2
2016/5/5	21	5.4	0.91	5.9	0.88	0.09	BDL	66	7.9	33	0.003	5921.03	2
2016/5/9	20	3.7	0.63	5.9	0.66	0.06	0.20	61	10	34	0.058	4461.39	2
2016/5/11	36	8.7	1.0	8.5	1.1	0.19	0.34	66	9.5	34	0.647	5327.31	2
2016/5/15	44	11	1.1	9.5	1.1	0.50	0.53	73	7.7	31	2.188	3869.72	1
2016/5/17	41	9.9	1.1	8.8	1.2	0.67	0.64	76	6.8	30	2.089	2627.67	1
2016/5/19	36	7.7	1.1	7.0	0.93	0.17	0.29	66	7.9	32	0.792	3161.86	1
2016/5/21	25	5.8	0.94	6.2	0.92	0.02	0	65	9.3	32	1.402	2336.95	6

2016/5/23	39	7.1	0.93	7.6	0.98	0.39	0	63	10	31	12.116	2166.24	6
2016/5/25	39	8.1	1.4	5.7	0.69	0.11	0.31	58	11	32	1.066	1400.26	6
2016/5/27	39	6.6	1.0	6.6	0.78	0.16	0.39	62	8.3	32	1.198	2902.14	6
2016/5/29	46	6.0	0.88	6.8	0.89	0.23	0.52	61	8.8	32	2.901	902.48	1
2016/5/31	42	7.9	1.2	6.8	0.84	0.05	0.41	82	7.5	29	2.012	1927.43	1
2016/6/2	41	7.3	1.3	5.7	0.92	0.05	0.40	80	6.3	30	1.046	2302.63	2
2016/6/14	37	7.9	1.3	5.9	0.68	0.00	0.26	68	8.1	31	0.363	2907.11	6
2016/10/22	18	5.4	1.2	4.6	0.49	0.26	0.07	73	8.9	30	3.326	2077.57	6
2016/10/24	26	6.2	1.1	5.7	0.72	0.70	0.25	73	6.7	29	1.569	3366.86	1
2016/10/26	17	5.8	1.2	4.9	0.61	0.12	0.09	89	5.4	28	6.510	2059.29	4
2016/10/28	30	7.4	1.5	5.1	0.71	0.19	0.25	84	5.9	29	1.616	3684.34	4
2016/10/30	18	5.8	1.0	5.6	0.47	0.09	0.08	89	5.0	27	5.517	2707.15	5
2016/11/1	26	8.9	1.3	7.1	0.73	0.12	BDL	82	6.1	29	0.203	2615.73	3
2016/11/3	40	10	1.6	6.5	0.92	0.35	0.39	75	5.2	28	1.372	3752.32	3
2016/11/5	75	17	1.9	9.1	1.3	1.1	1.4	70	4.3	29	0.001	3672.66	4
2016/11/7	60	12	2.3	5.4	1.2	1.2	1.4	80	3.2	29	9.042	787.82	4
2016/11/9	43	10	1.7	6.1	1.2	0.62	0.98	89	5.3	28	6.884	317.76	4
2016/11/13	49	14	1.7	8.6	1.2	0.19	0.57	75	6.3	29	3.125	4701.36	5
2016/11/15	44	12	1.3	9.1	1.5	BDL	BDL	72	5.8	30	0.028	4410.31	5
2016/11/17	62	12	1.3	9.4	0.99	0.12	0.45	67	7.4	29	0.000	7075.15	5
2016/11/19	46	11	1.1	9.6	1.2	0.42	0.61	74	6.3	29	1.836	2255.39	4
2016/11/21	93	24	1.6	15	1.5	0.46	0.90	73	5.8	30	0.581	3279.00	4
2016/11/23	57	13	1.2	11	1.1	0.25	0.48	75	6.4	29	10.938	1452.02	4
2016/11/25	64	15	2.3	6.5	0.95	0.25	0.57	83	4.9	29	0.156	3046.12	5
2016/11/27	41	9.3	0.96	9.6	0.75	0.15	0.23	69	5.6	29	0.130	1766.73	5

2016/11/29	78	15	1.5	10	0.92	0.44	0.82	71	4.6	27	0.000	5736.78	5
2016/12/1	66	12	1.4	8.5	0.97	0.49	0.48	68	6.0	27	0.002	5181.22	5
2016/12/3	64	12	1.3	9.2	0.88	0.45	0.56	67	8.2	28	0.012	2908.52	5
2016/12/5	51	14	1.3	11	1.3	0.41	0.33	72	5.1	28	0.614	2746.71	5
2016/12/7	73	14	1.5	9.4	1.7	0.67	0.56	65	6.5	27	0.931	2198.62	5
2016/12/9	103	21	2.1	10	1.4	0.91	1.1	65	4.2	27	0.000	5908.49	5
2016/12/11	106	24	1.8	13	1.7	1.7	1.2	62	6.2	27	0.021	3175.09	4
2016/12/13	98	25	1.9	13	1.3	0.86	1.2	60	7.3	27	0.005	4615.21	4
2016/12/15	46	9.2	0.85	11	0.75	0.09	0.22	68	8.8	28	5.802	1251.42	3
2016/12/17	81	17	1.3	13	1.5	0.43	0.93	62	7.5	25	0.179	929.87	5
2016/12/20	124	29	2.0	15	2.1	0.75	2.1	65	5.8	29	0.003	3904.70	5
2016/12/27	50	13	0.92	14	1.0	0.17	0.40	58	5.9	29	0.000	5351.00	3
2017/1/3	57	12	1.3	9.8	1.1	0.20	0.54	70	7.6	27	0.114	2825.05	3
2017/1/7	110	25	2.0	12	2.3	0.59	1.3	71	7.0	28	2.041	330.58	4
2017/1/14	90	20	1.9	10	1.7	0.50	0.80	75	4.7	29	0.599	3377.36	5
2017/1/21	66	14	1.1	13	1.0	0.30	0.87	62	6.1	29	0.000	3822.33	3
2017/1/28	98	22	1.8	12	1.6	0.50	1.2	55	5.1	27	0.000	5900.06	4

BDL: below detection limits.

Table S2. The concentration of TSP, carbonaceous aerosol, WSON, WSIN, and molecular markers in marine-, mixed-, and continental-influenced days.

	Marine (n = 36)		Mixed (n = 21)		Continental (n = 27)		All (n = 84)	
	Ave	SD	Ave	SD	Ave	SD	Ave	SD
TSP (μg m^{-3})	42	21	54	24	73	34	55	30
OC (μg m^{-3})	8.4	2.4	11	4.7	17	7.7	12	6.3
EC (μg m^{-3})	1.2	0.32	1.4	0.48	1.6	0.40	1.4	0.43
WSOC (μg m^{-3})	4.6	1.8	5.2	2.5	8.5	4.7	6.0	3.6
WSON (μgN m^{-3})	0.72	0.25	1.0	0.34	1.2	0.43	0.95	0.40
NH_4^+-N (μgN m^{-3})	0.42	0.38	0.27	0.25	0.68	0.56	0.47	0.44
NO_3^--N (μgN m^{-3})	0.40	0.28	0.53	0.39	0.93	0.68	0.60	0.52
Na^+ (μg m^{-3})	1.4	0.74	0.57	0.46	0.34	0.28	0.86	0.74
Cl^- (μg m^{-3})	0.27	0.16	0.20	0.14	0.21	0.10	0.23	0.14
*nss-K^+	0.49	0.16	0.49	0.25	0.77	0.45	0.58	0.33
*nss-SO_4^{2-}	5.5	2.9	2.9	2.0	4.0	2.6	4.0	2.6
Na^+/∑ions	0.11	0.040	0.060	0.038	0.028	0.023	0.028	0.023
OC/EC	8.1	7.2	8.4	2.4	10.1	3.0	8.9	5.2
WSOC/OC	0.54	0.11	0.44	0.08	0.49	0.08	0.50	0.10
WSON/WSOC	0.17	0.070	0.22	0.070	0.17	0.069	0.18	0.07
				Molecular tracers (ng m^{-3})				
Levoglucosan	70	54	140	112	337	282	174	207
Galactosan	2.3	1.4	4.9	3.6	11	8.2	5.6	6.17
Mannosan	5.8	3.8	9.2	6.3	17	12	10.3	9.29
Hopanes and steranes	1.2	0.4	1.3	0.7	1.3	0.7	1.3	0.60
2-MGA	3.2	1.5	5.0	2.6	6.6	4.1	4.8	3.2
2-MGL	36	22	29	17	38	23	35	21
MBTCA	11	7.2	31	22	29	12	22	17
o-Phthalic acid	7.9	4.4	4.1	3.4	7.5	7.3	6.8	5.5
p-Phthalic acid	10	7.9	31	25	43	26	26	25

nss: non-sea-salt

Table S3. The monthly averaged WSON concentration in the selected coastal cities that are impacted by marine air masses on a global scale and the corresponding AEC (air mass exposure to Chl a). The Chl a concentration was from the MODIS-Aqua (EARTHDATA, https://giovanni.gsfc.nasa.gov/giovanni/).

Sites	Data	Monthly averaged WSON (nmol m^{-3})	AEC (mg m^{-3})	References
Keelung City	2006/07	27.2	0.136	Chen and Chen (2010)
	2006/08	22.9	0.190	
South China Sea	2005/04	65	0.163	Shi et al. (2010)
Jiaozhou Bay, China	2015/07	190	0.860	Xing et al. (2018)
Hong Kong	2011/08	95	0.524	Ho et al. (2019)
	2011/09	95	0.319	
Hong Kong	2017/01	130.5	0.391	Leung et al. (2024)
	2017/03	114.7	0.306	
	2017/04	119.8	0.151	
	2017/05	117.0	0.230	
	2017/06	82.6	0.181	
	2017/07	114.8	0.250	
	2017/08	90.6	0.499	
	2017/09	93.3	0.445	
Eastern Mediterranean	2011/01	11.6	0.081	Tsagkaraki et al. (2021)
	2011/02	11.1	0.081	
	2011/04	9.45	0.118	
	2011/05	12.3	0.085	
	2011/06	22.2	0.071	
	2011/07	14.7	0.028	
	2011/08	16.4	0.082	
	2011/09	13.9	0.097	
	2011/10	8.12	0.073	
	2011/11	11.7	0.062	
	2011/12	9.71	0.081	
Okinawa Island	2010/06	34.6	0.068	Kunwar and Kawamura (2014)
	2010/07	2.88	0.030	
	2010/08	2.88	0.035	
	2010/09	5.77	0.048	

	2010/10	4.32	0.141	
Barbados	2008/08	3.5	0.038	Zamora et al. (2011)
Huaniao island	2019/07	231.30	0.505	Tian et al. (2023)
	2019/08	211.56	0.474	
Sapporo	2010/06	6.56	0.159	Pavuluri et al. (2015)
	2010/07	4.63	0.135	
	2010/08	1.54	0.125	
Bangkok, Thailand	2016/01	36.96	0.197	This study
	2016/02	81.96	0.377	
	2016/03	52.03	0.199	
	2016/04	46.30	0.238	
	2016/05	63.93	0.311	
	2016/06	57.39	0.321	

96

97

Table S4. The mapping of bootstrap (BS) factors and Fpeak BS factors to base factors for seven-factor solutions. (Number of bootstrap runs: 100)

		Factor 1	Factor 2	Factor 3	Factor 4	Factor 5	Factor 6	Factor 7	Unmapped
BS Mapping	Factor 1	100	0	0	0	0	0	0	0
	Factor 2	0	91	0	3	2	4	0	0
	Factor 3	0	1	96	1	0	1	1	0
	Factor 4	0	1	0	99	0	0	0	0
	Factor 5	0	0	2	0	98	0	0	0
	Factor 6	0	0	0	1	0	99	0	0
	Factor 7	1	0	1	2	1	0	95	0
Fpeak BC Mapping (Fpeak value - 0.5)	Factor 1	100	0	0	0	0	0	0	0
	Factor 2	0	92	2	3	1	2	0	0
	Factor 3	0	0	96	3	1	0	0	0
	Factor 4	0	0	1	97	2	0	0	0
	Factor 5	0	0	1	2	96	1	0	0
	Factor 6	0	0	0	2	0	98	0	0
	Factor 7	1	1	1	3	0	1	93	0

Table S5. Displacement (DISP) diagnostics of seven-factor solutions. Bootstrapping with displacement (BS-DISP) diagnostics of seven-factor solutions.

Constrained DISP Diagnostics:							
Error Code:	0						
%dQ:	-0.016758291						
Swaps by Factor:	0	0	0	0	0	0	0

Constrained BS-DISP Diagnostics:							
# of Cases:	81						
%dQ:	-0.106123702						
Swaps by Factor:	0	5	1	2	4	3	3

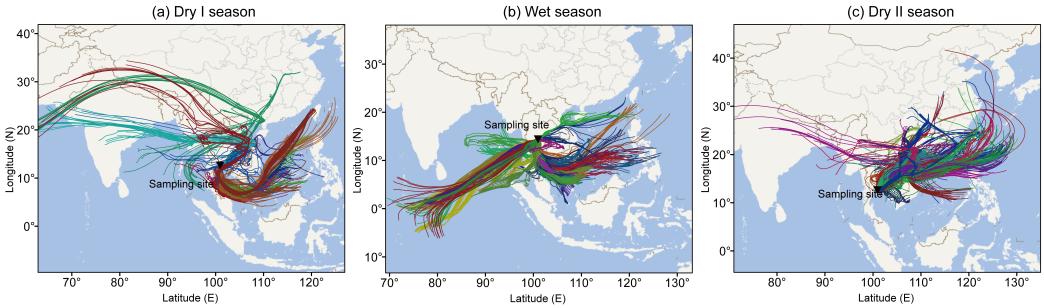

108

109 **Figure S1**. The 120 h back air-mass trajectories at Bangkok, Thailand, in the Dry I (a),
110 Wet (b), and Dry II seasons (c). The air mass trajectories were analyzed using the
111 HYSPLIT model. The map was created using ArcGIS software with the basemap from
112 the National Platform for Common Geospatial Information Services. Map source and
113 attribution: National Platform for Common Geospatial Information Services
114 (www.webmap.cn).

115

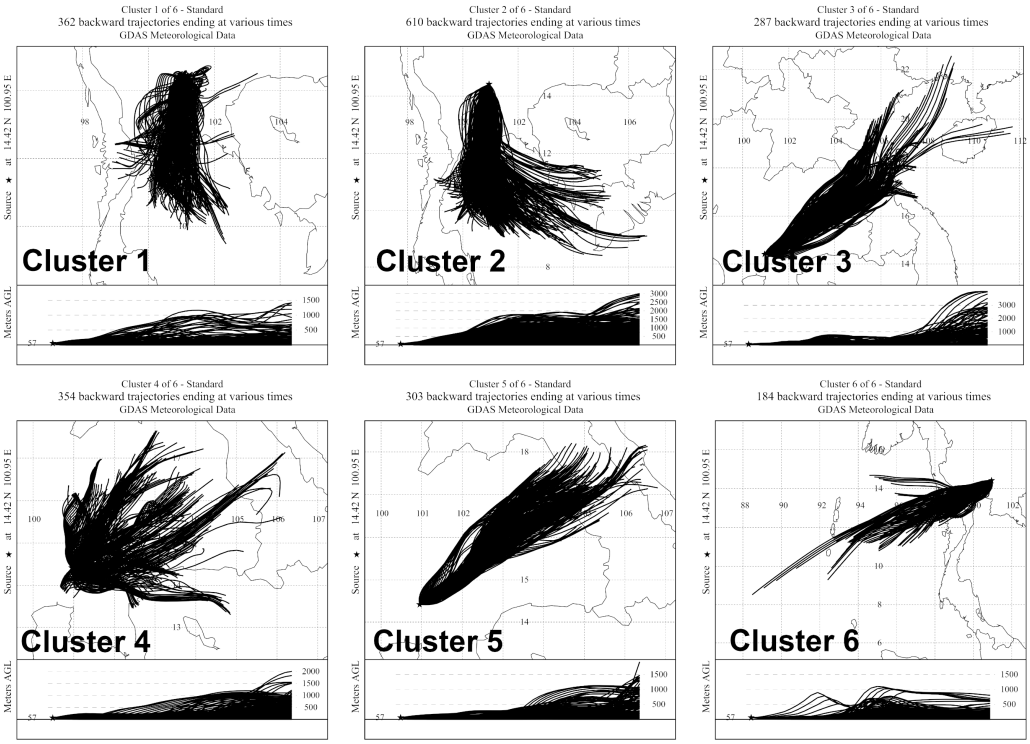

116

117 **Figure S2**. The 120 h back air-mass trajectories at Bangkok, from Thailand, during
118 January, 2016 to January, 2017. The backward trajectories were clustered into six
119 groups. The air mass trajectories were analyzed using the HYSPLIT model.

120

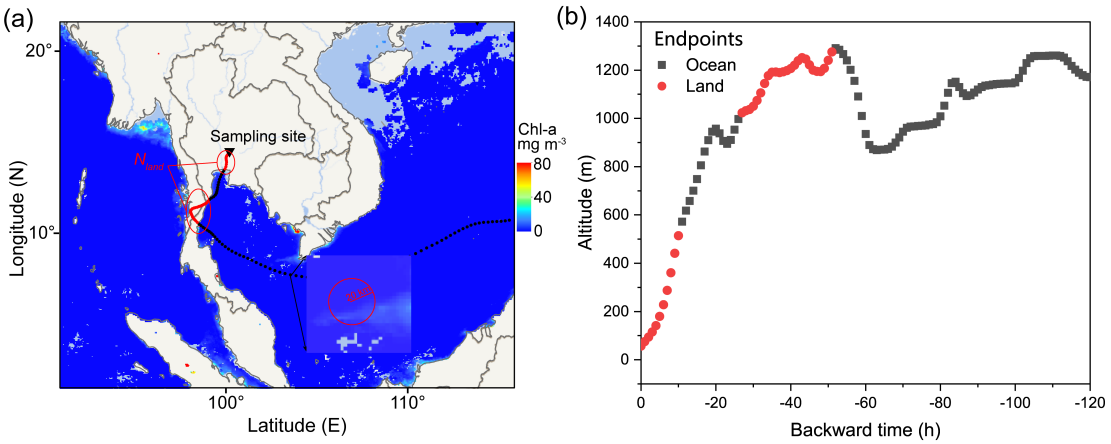

121

122 **Figure S3**. Schematic diagram of the calculations of (a) R_{land} and AEC, and (b) altitude
123 of each air-mass endpoints using120-hour trajectories. The red points refer to the air-
124 mass endpoints along trajectories located over the land. This 20 km radius was
125 representative of the area used as the search radius to compute the mean Chl-a
126 concentration at the air-mass endpoints.

127

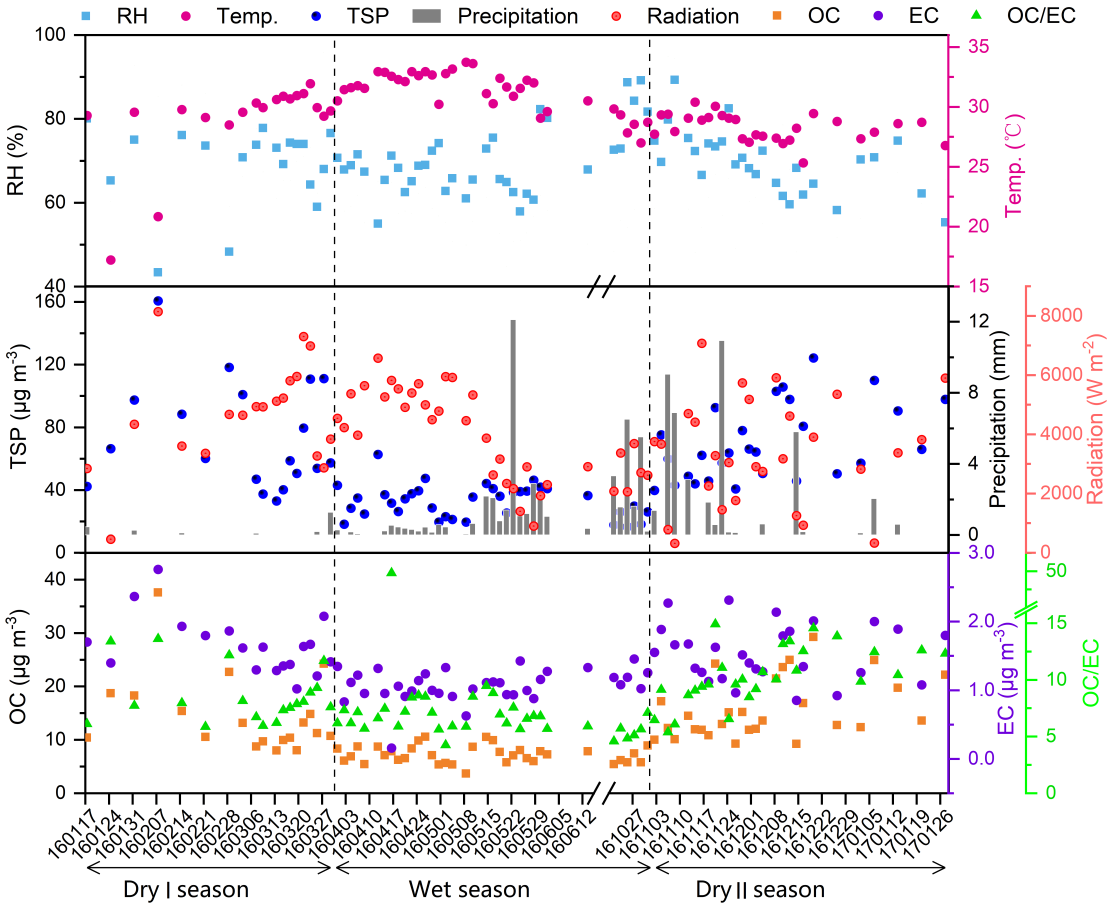

Figure S4. Meteorological data including relative humidity (RH), temperature (Temp.), precipitation, and radiation, along with time-series of TSP, OC, EC, and the ratio of OC/EC.

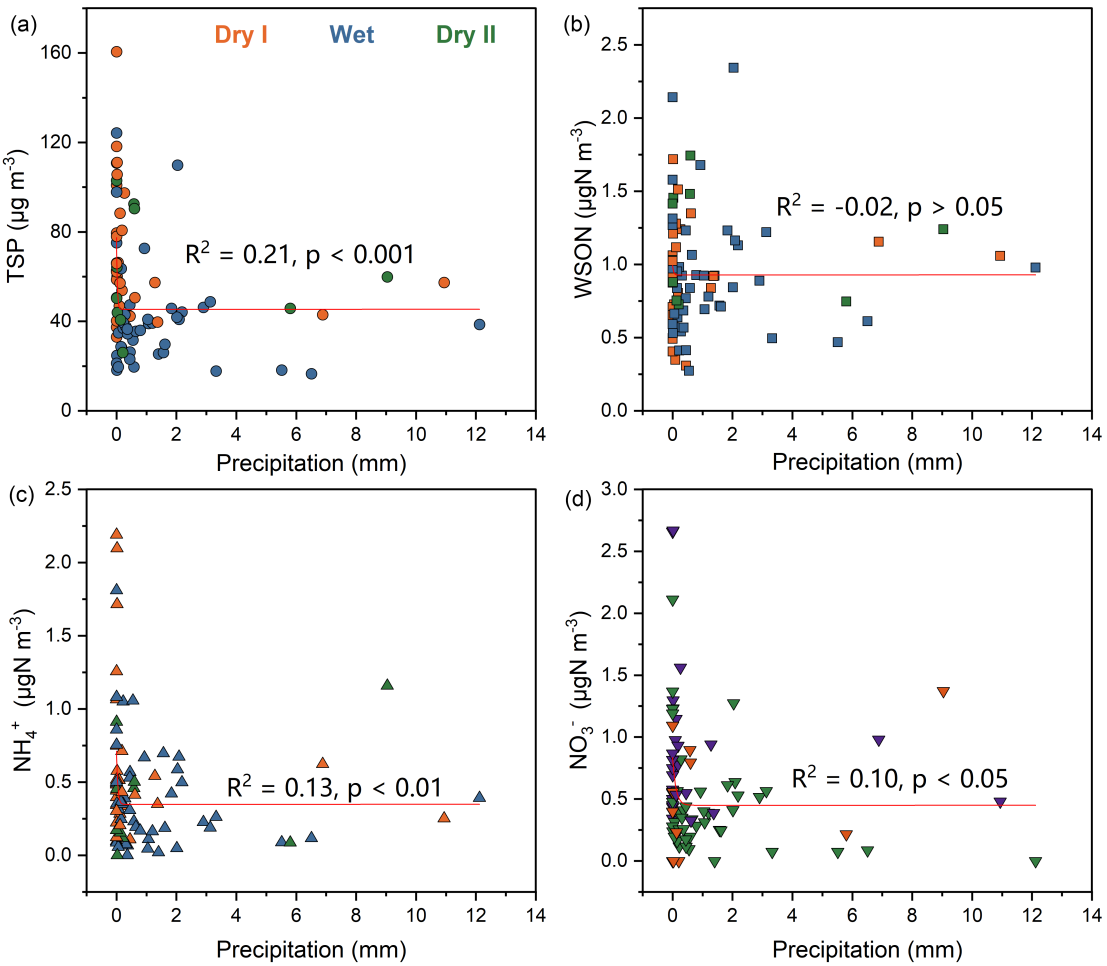

133

134 **Figure S5**. Exponential relationships between TSP (a), WSON (b), WSIN (c, d) and
135 precipitation.

136

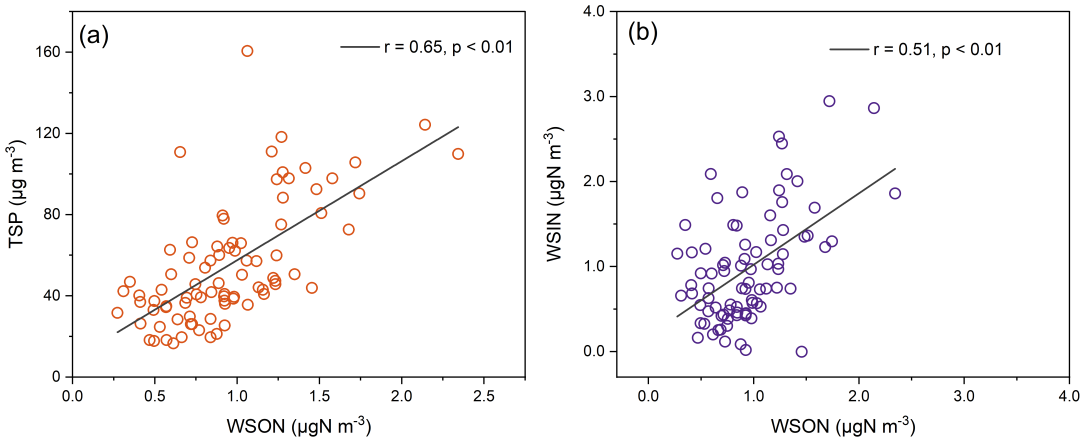

137

138 **Figure S6**. Linear relations of WSON to WSIN (sum of NO_3^--N and NH_4^+-N).

139

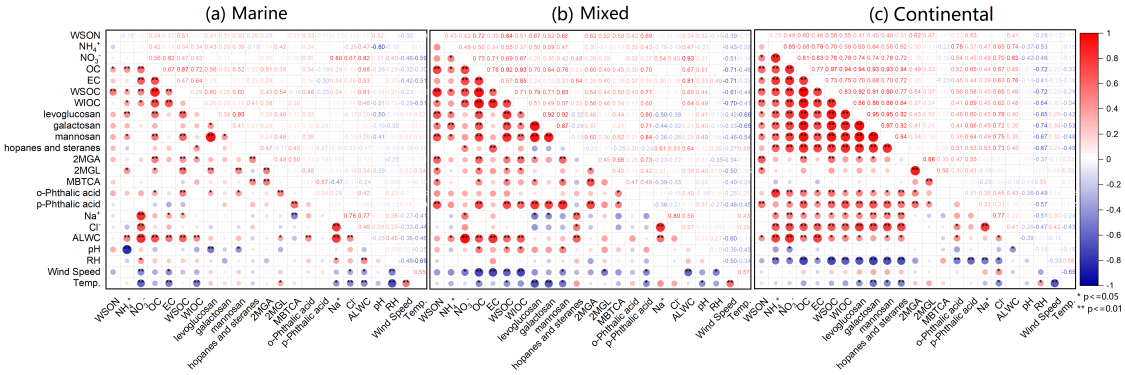

Figure S7. The correlation hotspots in marine- (a), mixed- (b), and continental-influenced days (c).

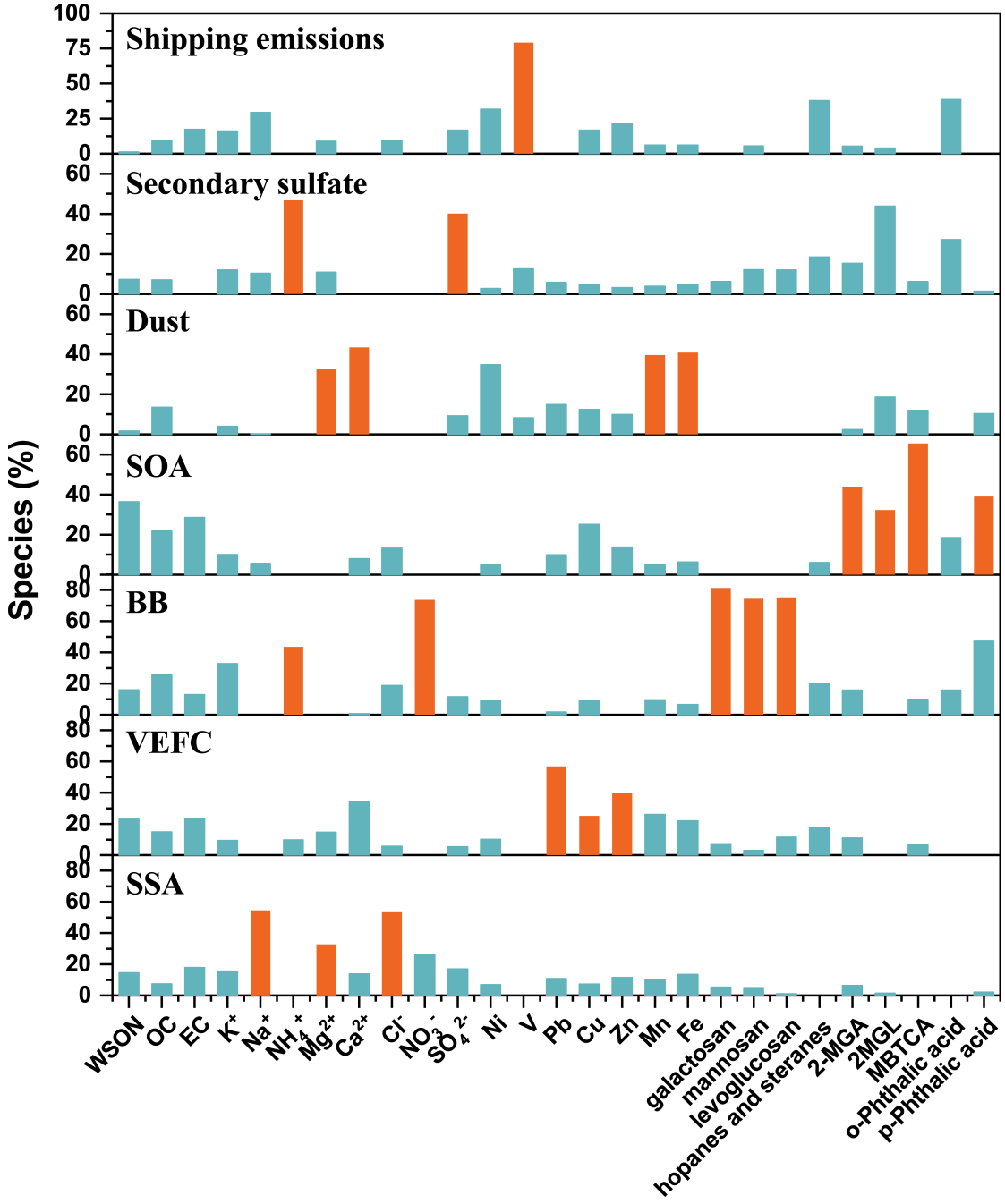

144

145 **Figure S8**. Seven factor profiles derived from the PMF solution. The percentage of
146 chemical species in each factor is shown.

147

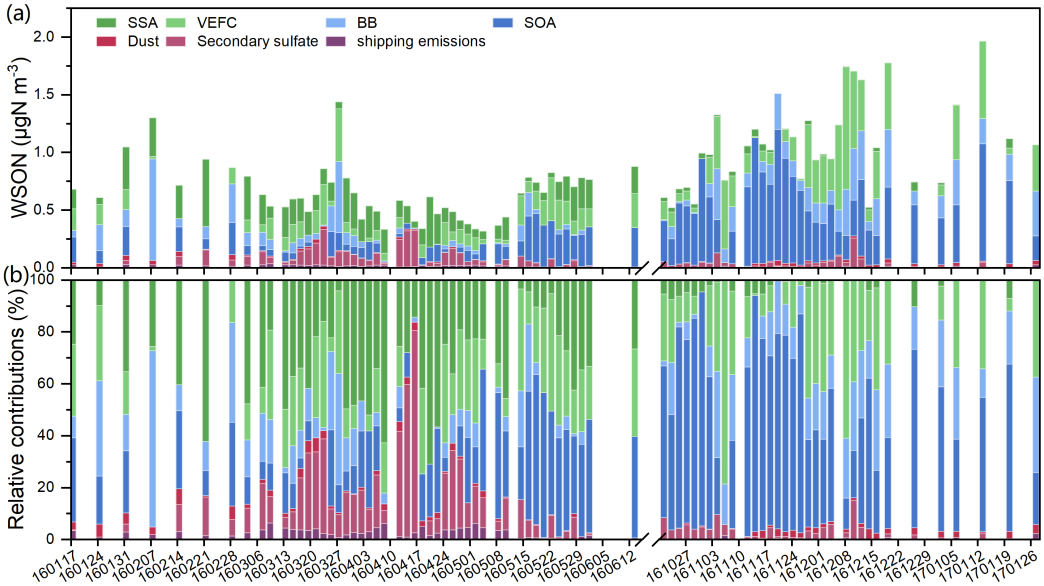

Figure S9. The time series of the seven PMF source factors and their relative contributions to WSON (a, b).

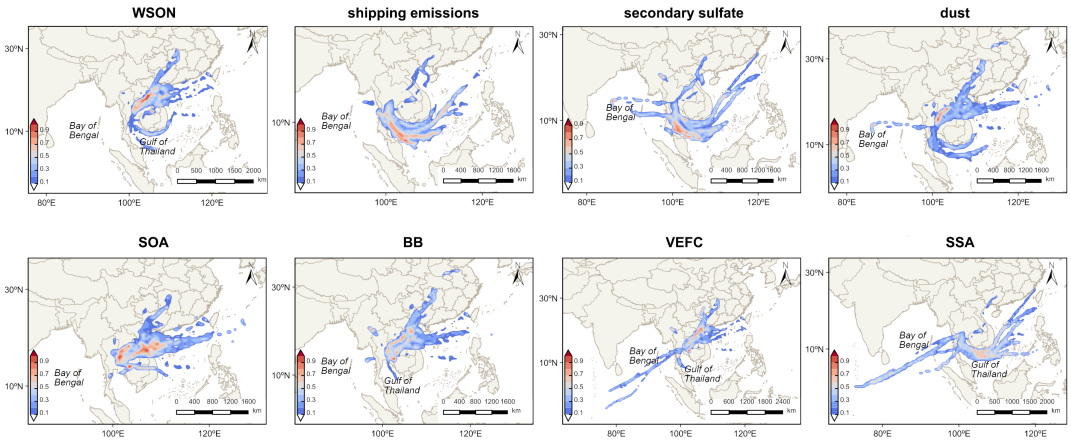

Figure S10. PSCF results of WSON and the seven-factor derived WSON resolved by PMF model. Threshold values were set as the 75th percentile of the corresponding values. The 120-hr backward air mass trajectory was analyzed using the HYSPLIT model.

References:

Celo, V., Dabek-Zlotorzynska, E., and McCurdy, M.: Chemical Characterization of Exhaust Emissions from Selected Canadian Marine Vessels: The Case of Trace Metals and Lanthanoids, Environ. Sci. Technol., 49, 5220-5226, https://doi.org/10.1021/acs.est.5b00127, 2015.

Chen, H.-Y., and Chen, L.-D.: Occurrence of water soluble organic nitrogen in aerosols at a coastal area, J. Atmos. Chem., 65, 49-71, https://doi.org/10.1007/s10874-010-9181-y, 2010.

Facchini, M. C., Rinaldi, M., Decesari, S., Carbone, C., Finessi, E., Mircea, M., Fuzzi, S., Ceburnis, D., Flanagan, R., Nilsson, E. D., de Leeuw, G., Martino, M., Woeltjen, J., and O'Dowd, C. D.: Primary submicron marine aerosol dominated by insoluble organic colloids and aggregates, Geophys. Res. Lett., 35, https://doi.org/10.1029/2008GL034210, 2008.

Fountoukis, C., and Nenes, A.: ISORROPIA II: a computationally efficient thermodynamic equilibrium model for K^+–Ca^{2+}–Mg^{2+}–NH_4^+–Na^+–SO_4^{2-}–NO_3^-–Cl^-–H_2O aerosols, Atmos. Chem. Phys., 7, 4639-4659, https://doi.org/10.5194/acp-7-4639-2007, 2007.

Geng, X., Mo, Y., Li, J., Zhong, G., Tang, J., Jiang, H., Ding, X., Malik, R. N., and Zhang, G.: Source apportionment of water-soluble brown carbon in aerosols over the northern South China Sea: Influence from land outflow, SOA formation and marine emission, Atmos. Environ., 229, 117484, https://doi.org/10.1016/j.atmosenv.2020.117484, 2020.

Ho, S. S. H., Li, L., Qu, L., Cao, J., Lui, K. H., Niu, X., Lee, S.-C., and Ho, K. F.: Seasonal behavior of water-soluble organic nitrogen in fine particulate matter ($PM_{2.5}$) at urban coastal environments in Hong Kong, Air Qual. Atmos. Health, 12, 389-399, https://doi.org/10.1007/s11869-018-0654-5, 2019.

Kunwar, B., and Kawamura, K.: One-year observations of carbonaceous and nitrogenous components and major ions in the aerosols from subtropical Okinawa Island, an outflow region of Asian dusts, Atmos. Chem. Phys., 14, 1819-1836, https://doi.org/10.5194/acp-14-1819-2014, 2014.

Leung, C. W., Wang, X., and Hu, D.: Characteristics and source apportionment of water-soluble organic nitrogen (WSON) in $PM_{2.5}$ in Hong Kong: With focus on amines, urea, and nitroaromatic compounds, J. Hazard. Mater., 469, 133899, https://doi.org/10.1016/j.jhazmat.2024.133899, 2024.

Li, X. G., Wang, S. X., Duan, L., Hao, J., Li, C., Chen, Y. S., and Yang, L.: Particulate and trace gas emissions from open burning of wheat straw and corn stover in

China, Environ. Sci. Technol., 41, 6052-6058, https://doi.org/10.1021/es0705137, 2007.

Pavuluri, C. M., Kawamura, K., and Fu, P. Q.: Atmospheric chemistry of nitrogenous aerosols in northeastern Asia: biological sources and secondary formation, Atmos. Chem. Phys., 15, 9883-9896, https://doi.org/10.5194/acp-15-9883-2015, 2015.

Petit, J. E., Favez, O., Albinet, A., and Canonaco, F.: A user-friendly tool for comprehensive evaluation of the geographical origins of atmospheric pollution: Wind and trajectory analyses, Environ. Modell. Softw., 88, 183-187, https://doi.org/10.1016/j.envsoft.2016.11.022, 2017.

Shi, J., Gao, H., Qi, J., Zhang, J., and Yao, X.: Sources, compositions, and distributions of water-soluble organic nitrogen in aerosols over the China Sea, J. Geophys. Res.-Atmos., 115, https://doi.org/10.1029/2009JD013238, 2010.

Tang, J., Xu, B., Zhao, S., Li, J., Tian, L., Geng, X., Jiang, H., Mo, Y., Zhong, G., Jiang, B., Chen, Y., Tang, J., and Zhang, G.: Long-Emission-Wavelength Humic-Like Component (L-HULIS) as a Secondary Source Tracer of Brown Carbon in the Atmosphere, J. Geophys. Res.-Atmos., 129, e2023JD040144, https://doi.org/10.1029/2023JD040144, 2024.

Tian, M., Li, H., Wang, G., Fu, M., Qin, X., Lu, D., Liu, C., Zhu, Y., Luo, X., Deng, C., Abdullaev, S. F., and Huang, K.: Seasonal source identification and formation processes of marine particulate water soluble organic nitrogen over an offshore island in the East China Sea, Sci. Total Environ., 863, 160895, https://doi.org/10.1016/j.scitotenv.2022.160895, 2023.

Tiwari, S., Kaskaoutis, D., Soni, V. K., Dev Attri, S., and Singh, A. K.: Aerosol columnar characteristics and their heterogeneous nature over Varanasi, in the central Ganges valley, Environ Sci Pollut Res Int, 25, 24726-24745, https://doi.org/10.1007/s11356-018-2502-4, 2018.

Tsagkaraki, M., Theodosi, C., Grivas, G., Vargiakaki, E., Sciare, J., Savvides, C., and Mihalopoulos, N.: Spatiotemporal variability and sources of aerosol water-soluble organic nitrogen (WSON), in the Eastern Mediterranean, Atmos. Environ., 246, 118144, https://doi.org/10.1016/j.atmosenv.2020.118144, 2021.

Viana, M., Amato, F., Alastuey, A., Querol, X., Moreno, T., García Dos Santos, S., Herce, M. D., and Fernández-Patier, R.: Chemical Tracers of Particulate Emissions from Commercial Shipping, Environ. Sci. Technol., 43, 7472-7477, https://doi.org/10.1021/es901558t, 2009.

Xing, J., Song, J., Yuan, H., Wang, Q., Li, X., Li, N., Duan, L., and Qu, B.: Water-soluble nitrogen and phosphorus in aerosols and dry deposition in Jiaozhou Bay, North China: Deposition velocities, origins and biogeochemical implications, Atmos.

Res., 207, 90-99, https://doi.org/10.1016/j.atmosres.2018.03.001, 2018.

Xu, B., Zhang, G., Gustafsson, Ö., Kawamura, K., Li, J., Andersson, A., Bikkina, S., Kunwar, B., Pokhrel, A., Zhong, G., Zhao, S., Li, J., Huang, C., Cheng, Z., Zhu, S., Peng, P., and Sheng, G.: Large contribution of fossil-derived components to aqueous secondary organic aerosols in China, Nat. Commun., 13, 5115, https://doi.org/10.1038/s41467-022-32863-3, 2022.

Zamora, L. M., Prospero, J. M., and Hansell, D. A.: Organic nitrogen in aerosols and precipitation at Barbados and Miami: Implications regarding sources, transport and deposition to the western subtropical North Atlantic, J. Geophys. Res.-Atmos., 116, https://doi.org/10.1029/2011JD015660, 2011.